Validity of standard model EFT studies of *VH* and *VV* production at NLO

Julien Baglio[,1,*] Sally Dawson[,2,†] Samuel Homiller[,3,‡] Samuel D. Lane,[2,4,§] and Ian M. Lewis[4,‖]

[1]*CERN, Theoretical Physics Department, CH-1211 Geneva 23, Switzerland*
[2]*Department of Physics, Brookhaven National Laboratory, Upton, New York 11973, USA*
[3]*C. N. Yang Institute for Theoretical Physics, Stony Brook University, Stony Brook, New York 11794, USA*
[4]*Department of Physics and Astronomy, University of Kansas, Lawrence, Kansas 66045, USA*

The production of $W^{\pm}H$, ZH, $W^{+}W^{-}$, and $W^{\pm}Z$ pairs probes non-Standard-Model interactions of quarks, gauge bosons, and the Higgs boson. New effects can be parametrized in terms of an effective field theory (EFT) where the Lagrangian is expanded in terms of higher-dimension operators suppressed by increasing powers of a high scale Λ. We examine the importance of including next-to-leading-order QCD corrections in global fits to the coefficients of the EFT. The numerical implications on the fits due to different approaches to enforcing the validity of the EFT are quantified. We pay particular attention to the dependence of the fits on the expansion in $1/\Lambda^2$ since the differences between results calculated at $\mathcal{O}(1/\Lambda^2)$ and $\mathcal{O}(1/\Lambda^4)$ may give insight into the possible significance of dimension-eight effects.

I. INTRODUCTION

One of the most interesting tasks of the high-luminosity phase of the LHC is to quantify possible experimental differences of Standard Model (SM) observables from the theoretical predictions. In the absence of the discovery of new light particles, effective field theories provide an efficient means of exploring new physics effects through precision measurements [1–5]. Deviations from the SM can be described in terms of the SM effective field theory (SMEFT) [6,7] which contains an infinite tower of higher-dimension operators constructed out of SM fields [including an $SU(2)$ Higgs doublet] that are invariant under the $SU(3) \times SU(2) \times U(1)$ gauge theory,

$$\mathcal{L} \sim \mathcal{L}_{\text{SM}} + \sum_{i,n>4} \frac{C_{i,n}}{\Lambda^{(n-4)}} O_{i,n}. \qquad (1)$$

The scale Λ is taken to generically represent the energy scale of some unknown UV complete theory and, assuming $\Lambda \gg M_Z$, the dominant effects typically come from the lowest dimension operators. In our study, we consider only

the dimension-six operators and use the Warsaw operator basis [8,9].

Fits to the coefficient functions are done by truncating the Lagrangian expansion at $\mathcal{O}(\frac{1}{\Lambda^2})$. In previous work, we studied $W^{+}W^{-}$ and $W^{\pm}Z$ production at the LHC in order to understand the numerical impact of including next-to-leading-order (NLO) QCD corrections in the fits to the coefficients [10–12]. Here, we extend the study to include $W^{\pm}H$ and ZH production [13] and compute the limits on the coefficient functions when the cross sections are systematically expanded to $\mathcal{O}(\frac{1}{\Lambda^2})$ and $\mathcal{O}(\frac{1}{\Lambda^4})$ at leading order (LO) NLO QCD in the SMEFT. We include anomalous 3-gauge boson couplings, anomalous gauge boson–Higgs couplings, and anomalous quark-gauge boson couplings. The SMEFT also includes interesting 4-point interactions of the form $q\bar{q}VH$ ($V = W^{\pm}, Z$), which lead to novel features. Our work uses the implementation of these processes [11–16] in the POWHEG-BOX framework [17,18], and we include both 8 TeV and 13 TeV LHC data in the fits.

Gauge/Higgs boson pair production has been extensively studied in the SM. Higher-order SM QCD corrections for $W^{+}W^{-}$, $W^{\pm}Z$, $W^{\pm}H$, and ZH exist to NLO [19–31] and next-to-next-to-leading order [32–38], while electroweak corrections are known to NLO [39–46] for the various processes. The precisely known SM results rely on the properties of the SM couplings that give cancellations between Feynman diagrams such that the physical amplitudes do not grow with energy. Deviations from the SM interactions will spoil these cancellations [47,48], potentially giving measurable effects—especially in high-energy bins—and this property is exploited in the SMEFT fits. Higher-order QCD corrections, including effects of the

*julien.baglio@cern.ch
†dawson@bnl.gov
‡samuel.homiller@stonybrook.edu
§samuel.lane@ku.edu
‖ian.lewis@ku.edu

anomalous triple-gauge-boson couplings, exist at NLO for diboson production [49–52] and have been extended to include also the effect of anomalous quark couplings [10–12]. $W^{\pm}H$ and ZH channels are also known at NLO QCD including SMEFT operators [13,30,31,53,54].

In this work, we perform a fit to the dimension-six coefficients relevant for the W^+W^-, $W^{\pm}Z$, $W^{\pm}H$, and ZH channels at NLO QCD. At NLO, the additional jet reduces the sensitivity to anomalous couplings and this effect is often compensated for by imposing a jet veto above some p_T. Our focus is on understanding the numerical importance of the NLO SMEFT QCD corrections and the jet veto cuts on the sensitivity to the SMEFT coefficients [53,55].

Since we are considering dimension-six operators, the Lagrangian of Eq. (1) generates terms of $\mathcal{O}(\text{Energy}^2/\Lambda^2)$. If there is some generic coupling strength, g_{EFT}, associated with the EFT, there are also terms of $\mathcal{O}((g_{\text{EFT}}v)^2/\Lambda^2)$. For a weak-coupling EFT expansion to be valid, both classes of terms must be small. We study the regions in our fits where these criteria are satisfied [56]. We further study the numerical effects of including $1/\Lambda^2$ or $1/\Lambda^4$ contributions. It has been suggested that the difference between results obtained at $1/\Lambda^2$ or $1/\Lambda^4$ could be an indication of the size of the dimension-eight contributions, which are also formally of $\mathcal{O}(1/\Lambda^4)$ [57,58].

In Sec. II, we review the details of the SMEFT that are relevant for our study and the implementation in the POWHEG-BOX framework. Section III demonstrates the effects of NLO corrections on distributions and the effects of jet veto cuts on the sensitivity of these distributions to anomalous couplings. Finally, Sec. IV presents the results of both profiled and projected fits, while quantifying the effects of the NLO corrections, the effects of order $1/\Lambda^4$ on the fits, and a discussion of the applicability of our fits in the context of a weakly-coupled theory.

II. BASICS

The production rates for W^+W^-, $W^{\pm}Z$, $W^{\pm}H$, and ZH at high energy are extremely sensitive to new-physics effects

[3,59–63]. We parametrize possible new interactions in terms of general CP-conserving, Lorentz-invariant interactions, neglecting dipole interactions since they do not interfere with the SM results for these processes. We also neglect flavor effects. The correspondence between various SMEFT basis choices is straightforward [64], and we will always use the Warsaw basis for which the Feynman rules and operator definitions can be obtained from [65,66].

In the Warsaw basis, the relationships between inputs are altered from those of the SM. Taking the measured values of G_F, M_W, and M_Z as inputs, the tree-level shifts in the couplings are [66]

$$\frac{\delta G_F}{G_F} = \frac{v^2}{\Lambda^2}\left\{C_{Hl}^{(3)} - \frac{1}{2}C_{ll}\right\},$$

$$\frac{\delta M_Z^2}{M_Z^2} = \frac{v^2}{2\Lambda^2}\left\{C_{HD} + \frac{4M_W}{M_Z}\sqrt{1 - \frac{M_W^2}{M_Z^2}}C_{HWB}\right\},$$

$$\frac{\delta M_W^2}{M_W^2} = 0,$$

$$\delta g_Z = -\frac{v^2}{\Lambda^2}\left(\delta v + \frac{1}{4}C_{HD}\right),$$

$$\delta v = C_{Hl}^{(3)} - \frac{1}{2}C_{ll},$$

$$\delta s_W^2 = -\frac{v^2}{\Lambda^2}\frac{s_W c_W}{c_W^2 - s_W^2}\left[2s_W c_W\left(\delta v + \frac{1}{4}C_{HD}\right) + C_{HWB}\right],$$

where we write the SMEFT quantity x in terms of the measured value $\hat{x}$ and the shift δx: $x = \hat{x} - \delta x$. It should be noted that δv does not follow this method. Instead, it is the dimensionless shift to G_F coming from muon decay. With these inputs, $g^2 = 4\sqrt{2}G_F M_W^2$, $\cos\theta_W \equiv c_W = M_W/M_Z$, and $e = g\sin\theta_W \equiv gs_W$. In our fits we will take $C_{Hl}^{(3)} = \frac{1}{2}C_{ll} = 0$, since these parameters are tightly constrained by muon decays [67].

Historically, the SMEFT interactions have been studied from a general interaction perspective. The 3-gauge boson vertices can be written as

$$\mathcal{L}_{WWZ} = -ig_{WWZ}\left[g_1^Z(W_{\mu\nu}^+W^{-\mu}Z^\nu - W_{\mu\nu}^-W^{+\mu}Z^\nu) + \kappa^Z W_\mu^+W_\nu^- Z^{\mu\nu} + \frac{\lambda^Z}{M_W^2}W_{\rho\mu}^+W^{-\mu}{}_\nu Z^{\nu\rho}\right],$$

$$\mathcal{L}_{WW\gamma} = -ig_{WW\gamma}\left[(W_{\mu\nu}^+W^{-\mu}\gamma^\nu - W_{\mu\nu}^-W^{+\mu}\gamma^\nu) + \kappa^\gamma W_\mu^+W_\nu^-\gamma^{\mu\nu} + \frac{\lambda^\gamma}{M_W^2}W_{\rho\mu}^+W^{-\mu}{}_\nu\gamma^{\nu\rho}\right], \quad (2)$$

with $g_{WW\gamma} = e$, $g_{WWZ} = g\cos\theta_W$, $g_1^Z = 1 + \delta g_1^Z$, and $\kappa^{Z,\gamma} = 1 + \delta\kappa^{Z,\gamma}$. $SU(2)$ gauge invariance implies

$$\delta g_1^Z = \delta\kappa^Z + \frac{s_W^2}{c_W^2}\delta\kappa^\gamma,$$

$$\lambda^\gamma = \lambda^Z. \quad (3)$$

Expressions for the anomalous gauge couplings in the Warsaw basis are given in Table I [10,65,68,69].

TABLE I. Anomalous 3-gauge-boson couplings in the Warsaw basis. δv is given in Eq. (2).

	Warsaw basis
δg_1^Z	$\frac{v^2}{\Lambda^2}\frac{1}{c_W^2 - s_W^2}(\frac{s_W}{c_W}C_{HWB} + \frac{1}{4}C_{HD} + \delta v)$
$\delta \kappa^Z$	$\frac{v^2}{\Lambda^2}\frac{1}{c_W^2 - s_W^2}(2s_W c_W C_{HWB} + \frac{1}{4}C_{HD} + \delta v)$
$\delta \kappa^\gamma$	$-\frac{v^2}{\Lambda^2}\frac{c_W}{s_W}C_{HWB}$
λ^γ	$\frac{v}{\Lambda^2}3M_W C_W$
λ^Z	$\frac{v}{\Lambda^2}3M_W C_W$

Neglecting dipole interactions, the quark-gauge boson couplings can be written as

$$\mathcal{L}_{ffV} \equiv g_Z Z_\mu [g_L^{Zq} + \delta g_L^{Zq}]\bar{q}_L \gamma_\mu q_L + g_Z Z_\mu [g_R^{Zq} + \delta g_R^{Zq}]\bar{q}_R \gamma_\mu q_R$$
$$+ \frac{g}{\sqrt{2}}\{W_\mu[(1 + \delta g_L^W)\bar{u}_L \gamma_\mu d_L + \delta g_R^W \bar{u}_R \gamma_\mu d_R] + \text{H.c.}\},$$
$$(4)$$

where $\mathcal{L}_H^{\text{SM}}$ contains the relevant SM Higgs interactions. In the Warsaw basis, the effects of d_{2W} and d_{2Z} are eliminated using the equations of motion. Expressions for the anomalous Higgs couplings are given in the Warsaw basis in Table III [65]. Finally, the SMEFT contains two 4-point operators that contribute to VH production, $O_{Hq}^{(1)}$ and $O_{Hq}^{(3)}$ [65]. We note that the parametrizations of Eqs. (2)–(6) are closely related to those of the Higgs basis [71,72]. Finally, we assume that the $Hb\bar{b}$ coupling is SM-like, since we expect the anomalous coefficients involving the b and the Higgs to be suppressed by factors of $\frac{m_b}{v}$ compared to the effects of other operators.

with $g_Z = e/(c_W s_W) = g/c_W$. In the POWHEG implementations that we use later, neither the dipole interactions nor the right-handed quark couplings are implemented. These contributions first arise at $\mathcal{O}(1/\Lambda^4)$ and are of interest for future work, although beyond the scope of this study. Reference [70] demonstrated, however, that the inclusion of light quark dipole operators does not spoil the bounds extracted on gauge boson self-couplings from LHC data. The SM quark interactions are

$$g_R^{Zq} = -s_W^2 Q_q \quad \text{and} \quad g_L^{Zq} = T_3^q - s_W^2 Q_q, \quad (5)$$

where $T_3^q = \pm\frac{1}{2}$ and Q_q is the electric charge. Expressions for the anomalous fermion- gauge couplings in the Warsaw basis are given in Table II [10,65,68,69].

Finally, the relevant Higgs couplings (again neglecting dipole interactions) are described by

$$\mathcal{L}_{VVH} = \mathcal{L}_H^{\text{SM}} + d_{1Z}HZ_\mu Z^\mu + d_{2Z}Z_{\mu\nu}Z^\mu \partial^\nu H + d_{3Z}HZ_{\mu\nu}Z^{\mu\nu}$$
$$+ d_{1W}HW_\mu^+ W^{-\mu} + d_{2W}(W_{\mu\nu}^+ W^{-\mu} + W_{\mu\nu}^- W^{+\mu})\partial^\nu H + d_{3W}HW_{\mu\nu}W^{\mu\nu}$$
$$+ d_{1Z}^{Lf}(\bar{f}_L \gamma_\mu f_L)Z^\mu H + d_{1Z}^{Rf}(\bar{f}_R \gamma_\mu f_R)Z^\mu H$$
$$+ \{d_{1W}^L(\bar{u}_L \gamma_\mu d_L)W^\mu H + d_{1W}^R(\bar{u}_R \gamma_\mu d_R)W^\mu H + \text{H.c.}\},$$
$$(6)$$

We are now ready to count the parameters appearing in our study. The $W^+ W^-$ and WZ processes can be described by seven independent couplings that we take to be

TABLE III. Anomalous Higgs gauge boson couplings in the Warsaw basis.

	Warsaw basis
d_{1W}	$2M_W^2\sqrt{G_F\sqrt{2}}\{\frac{v^2}{\Lambda^2}(C_{H\square} - \frac{1}{4}C_{HD}) + \frac{\delta M_W^2}{M_W^2} + \frac{\delta G_F}{2G_F}\}$
d_{1Z}	$2M_Z^2\sqrt{G_F\sqrt{2}}\{\frac{v^2}{\Lambda^2}(C_{H\square} + \frac{3}{8}C_{HD} + s_W c_W C_{HWB}) + \frac{\delta M_Z^2}{M_Z^2} + \frac{\delta G_F}{2G_F}\}$
d_{3W}	$\frac{vC_{HW}}{\Lambda^2}$
d_{3Z}	$\frac{v}{\Lambda^2}(c_W^2 C_{HW} + s_W^2 C_{HB} + s_W c_W C_{HWB})$
d_{1Z}^{Ru}	$\frac{2M_Z}{\Lambda^2}C_{Hu}$
d_{1Z}^{Lu}	$\frac{2M_Z}{\Lambda^2}(C_{Hq}^{(1)} - C_{Hq}^{(3)})$
d_{1Z}^{Rd}	$\frac{2M_Z}{\Lambda^2}C_{Hd}$
d_{1Z}^{Ld}	$\frac{2M_Z}{\Lambda^2}(C_{Hq}^{(1)} + C_{Hq}^{(3)})$
d_{1W}^R	$-\sqrt{2}\frac{M_W}{\Lambda^2}C_{Hud}$
d_{1W}^L	$-2\sqrt{2}\frac{M_W}{\Lambda^2}C_{Hq}^{(3)}$

TABLE II. Anomalous fermion couplings in the Warsaw basis.

	Warsaw basis
δg_L^{Zu}	$-\frac{v^2}{2\Lambda^2}(C_{Hq}^{(1)} - C_{Hq}^{(3)}) + \frac{1}{2}\delta g_Z + \frac{2}{3}(\delta s_W^2 - s_W^2 \delta g_Z)$
δg_L^{Zd}	$-\frac{v^2}{2\Lambda^2}(C_{Hq}^{(1)} + C_{Hq}^{(3)}) - \frac{1}{2}\delta g_Z - \frac{1}{3}(\delta s_W^2 - s_W^2 \delta g_Z)$
δg_R^{Zu}	$-\frac{v^2}{2\Lambda^2}C_{Hu} + \frac{2}{3}(\delta s_W^2 - s_W^2 \delta g_Z)$
δg_R^{Zd}	$-\frac{v^2}{2\Lambda^2}C_{Hd} - \frac{1}{3}(\delta s_W^2 - s_W^2 \delta g_Z)$
δg_L^W	$\frac{v^2}{\Lambda^2}C_{Hq}^{(3)} + c_W^2 \delta g_Z + \delta s_W^2$

$$\delta g_1^Z, \quad \delta \kappa_Z, \quad \delta \lambda_Z, \quad \delta g_L^{Zu}, \quad \delta g_L^{Zd}, \quad \delta g_R^{Zu}, \quad \delta g_R^{Zd}. \qquad (7)$$

Neglecting possible right-handed W couplings (since they are known to be small [73]), the $W^\pm H$ process depends on three combinations of couplings,

$$d_{1W}, \quad d_{3W}, \quad C_{Hq}^{(3)}, \qquad (8)$$

where d_{1W} and d_{3W} are the couplings defined in Eq. (6) and Table III and $C_{Hq}^{(3)}$ is the Wilson coefficient for $O_{Hq}^{(3)}$. ZH production is sensitive to

$$d_{1Z}, \quad d_{3Z}, \quad \delta g_L^{Zu}, \quad \delta g_L^{Zd}, \quad \delta g_R^{Zu}, \quad \delta g_R^{Zd}, \quad (C_{Hq}^{(1)}, C_{Hq}^{(3)}), \qquad (9)$$

where d_{1Z} and d_{3Z} are defined in Eq. (6) and Table III and $(C_{Hq}^{(1)}, C_{Hq}^{(3)})$ is the combination of these Wilson coefficients that affects ZH production. Since we fit to $W^+ W^-, W^\pm Z, W^\pm H$, and WZ there are ten relevant parameters that we express in terms of their Warsaw basis coefficients. We note that the purpose of our study is not to do a complete global fit, but to quantify the effects of the QCD corrections and the expansion in powers of $1/\Lambda^2$ on fits to these observables.

III. RESULTS

A. Simulation

For each process ($W^+ W^-, W^\pm Z, W^\pm H$, and ZH), we introduce anomalous couplings in the Warsaw basis and utilize existing implementations in the POWHEG-BOX framework, working to NLO QCD within the SMEFT.[1] We consider only the leptonic decays of the gauge bosons and the Higgs decay to $b\bar{b}$. Using the POWHEG-BOX-V2 program, we compute primitive differential cross sections that allow us to scan over anomalous couplings in an efficient manner [10]. The primitive cross sections are extracted in such a way as to allow for the consistent calculation of cross sections at either linear, $\mathcal{O}(\frac{1}{\Lambda^2})$, or quadratic, $\mathcal{O}(\frac{1}{\Lambda^4})$, order. The results shown in the following sections use CTEQ14qed PDFs [75], and we fix the renormalization/factorization scales to $M_Z/2$.

Our results are calculated using the dimension-six SMEFT Lagrangian,

$$L = L_{SM} + \Sigma_i \frac{C_i^6}{\Lambda^2} O_i^6. \qquad (10)$$

Using the dimension-six Lagrangian, the amplitudes for the $2 \to 2$ processes considered here can be written as

$$A = A_{SM} + \Sigma_i \frac{C_i}{\Lambda^2} A_i^6 + \Sigma_{ij} \frac{C_i C_j}{\Lambda^4} A_{ij}^6, \qquad (11)$$

where A_{SM} is the SM amplitude. When squaring this amplitude, terms are generated of $\mathcal{O}(\frac{1}{\Lambda^2}), ..., \mathcal{O}(\frac{1}{\Lambda^8})$, and we systematically truncate the cross sections at either $\mathcal{O}(\frac{1}{\Lambda^2})$ or $\mathcal{O}(\frac{1}{\Lambda^4})$ when presenting our results. We note that the terms of $\mathcal{O}(\frac{1}{\Lambda^4})$ are formally of the same size as the neglected terms coming from the dimension-eight Lagrangian and that this is an inherent assumption in applying the dimension-six Lagrangian.

B. Distributions in the presence of radiation

A principal advantage of the SMEFT framework is that it allows for a systematic study of distributions in the presence of new physics modifying the couplings between the SM fields. An important goal is thus to understand how to extract the maximum possible amount of information from these distributions. In this light, it is crucial to understand how these distributions are influenced by higher-order corrections, particularly in the presence of extra QCD radiation. The presence of additional jets can substantially change the distributions, washing out effects present at tree level, and in some cases, dramatically change the results of a fit to experimental data [10–12]. The effects of a jet veto have been studied in the past by considering extra partons at the matrix element level at leading order [55,60] and at NLO QCD in the SM [53]. Our study includes the full NLO QCD SMEFT corrections and clearly demonstrates the difference between including $1/\Lambda^2$ terms and $1/\Lambda^4$ contributions in the cross sections.

The effects of NLO QCD corrections in the SMEFT on distributions with anomalous couplings in $W^+ W^-$ and $W^\pm Z$ production have been studied in previous work [10–12]. We now extend that analysis to include $W^\pm H$ and ZH production [13]. For $W^+ W^-$ production, it was demonstrated in Refs. [10–12] that the K factor—defined as the ratio of the NLO QCD (differential) cross section to the LO one—was largely unchanged by the presence of anomalous gauge and fermion couplings. For $W^\pm Z$ production, however, the effects of anomalous couplings on the K factor were found to be quite large. This can be understood as the result of a delicate cancellation between the tree-level diagrams leading to $W^\pm Z$ production in the SM, which are intimately related to the presence of an approximate radiation zero [76] in the tree-level amplitude. The radiation zero is spoiled by the presence of QCD radiation, leading to large K factors [39] in some differential distributions. Because anomalous couplings affect the cancellation between the tree-level diagrams, the interplay of radiation and anomalous couplings makes an understanding of the NLO predictions crucial to obtain accurate predictions of the distributions at the LHC.

---

[1]This public tool can be found at http://powhegbox.mib.infn.it. We make use of the WWanomal, WZanomal, HW_smeft and HZ_smeft user processes introduced in previous works [11–13,74].
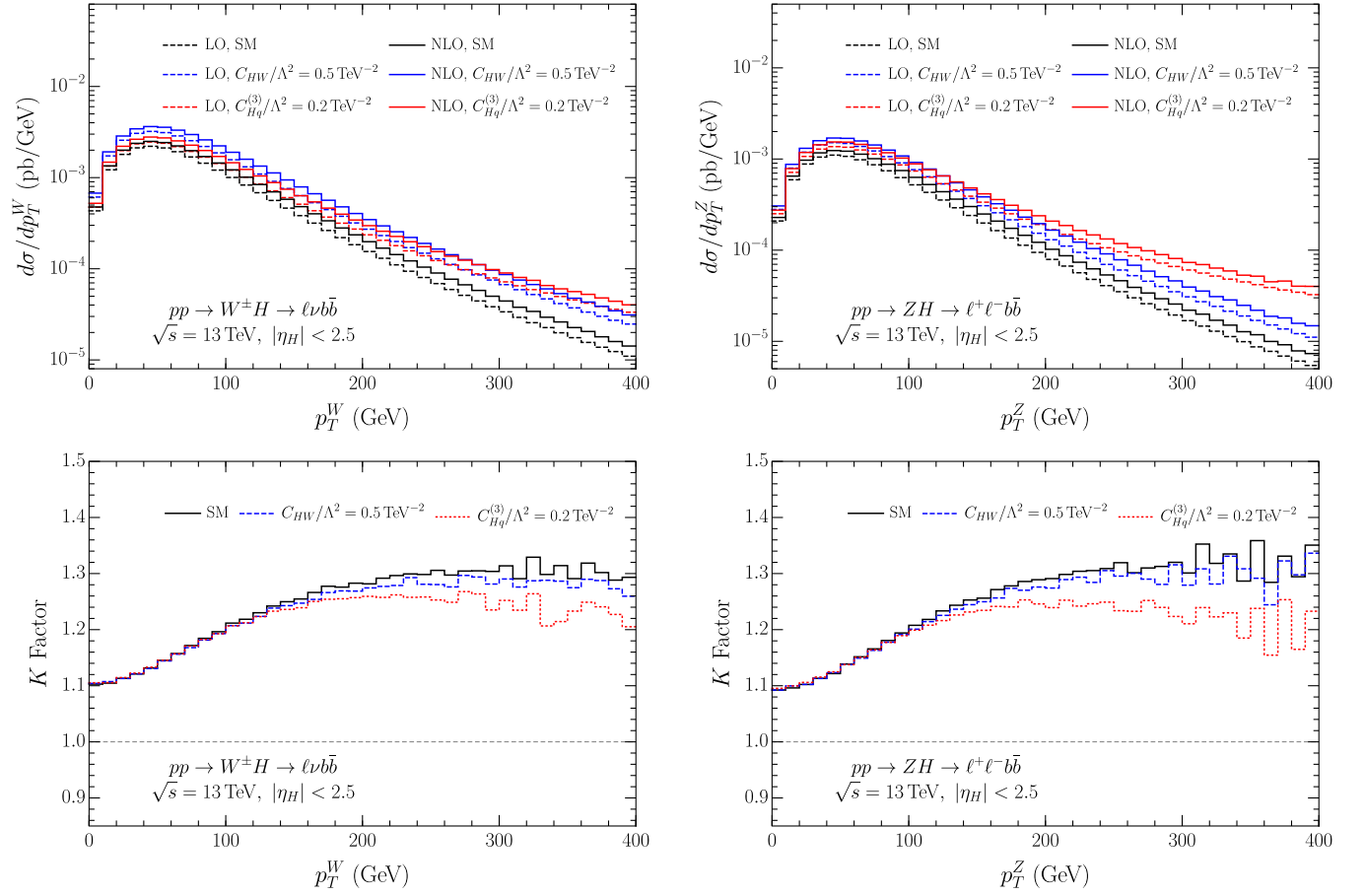
FIG. 1.   Top: Differential distributions for $W^{\pm}H$ (left) and ZH (right) production at LO (dashed lines) and NLO (solid lines) in bins of p_T^V. We plot the results for the SM (black lines), $C_{HW}/\Lambda^2 = 0.5$ TeV^{-2} (blue lines), and $C_{Hq}^{(3)}/\Lambda^2 = 0.2$ TeV^{-2} (red lines). Bottom: The associated K factors for the same distributions at the same three points, also in bins of p_T^V. The figures are computed to $\mathcal{O}(1/\Lambda^4)$.

We now consider the interplay of QCD corrections and anomalous couplings on differential distributions for the associated production of a Higgs and a $W^{\pm}$ or Z gauge boson [53,54]. While $W^{\pm}H$ and ZH production do not have a tree-level radiation zero as in $W^{\pm}Z$ production, the longitudinal modes at high energy are closely related to the W^+W^- and $W^{\pm}Z$ processes in the high-energy limit by the Goldstone theorem [3,77] and so we expect interesting effects from QCD radiation.

In Fig. 1, we show the differential cross sections for $W^{\pm}H$ and ZH production in bins of p_T^V for the Standard Model and with $C_{HW}/\Lambda^2 = 0.5$ TeV^{-2} (blue lines) and $C_{Hq}^{(3)}/\Lambda^2 = 0.2$ TeV^{-2} (red lines). This figure includes the differential cross sections evaluated to $\mathcal{O}(\frac{1}{\Lambda^4})$. The NLO and LO predictions are shown as solid and dashed lines, respectively. In the lower panels, we show the corresponding K factors at these benchmark points. At both LO and NLO, we see that the effects of $C_{Hq}^{(3)}$ grow fastest at high energy, due to the 4-point interaction being unsuppressed by an s-channel vector boson propagator [2,78]. For the

anomalous-coupling points and for the SM, for both $W^{\pm}H$ and ZH production, the K factor becomes larger at high p_T^V, reaching ~ 1.3 for the SM at 400 GeV. While less pronounced than the effects in $W^{\pm}Z$ production, treating the SMEFT contributions consistently at NLO QCD in the SMEFT changes the ratio of the NLO to LO predictions, and this has an effect on the fits to the distributions as we show in Sec. IV.

C. Angular distributions and gauge boson polarizations at NLO

We now turn to a discussion of the angular variables, $\cos\theta_W^*$ of the decayed charged leptons in the gauge boson rest frame. For $W^{\pm}Z$ production, we make use of the helicity coordinate system defined by ATLAS in Ref. [79], defining the z direction of the $W^{\pm}$ rest frame by the $W^{\pm}$ direction in the diboson center-of-mass frame. More details are given in Refs. [44,80]. For $W^{\pm}H$ and ZH production, we use the same variables, with the $W^{\pm}H$ or ZH system replacing the $W^{\pm}Z$ center-of-mass frame, and the
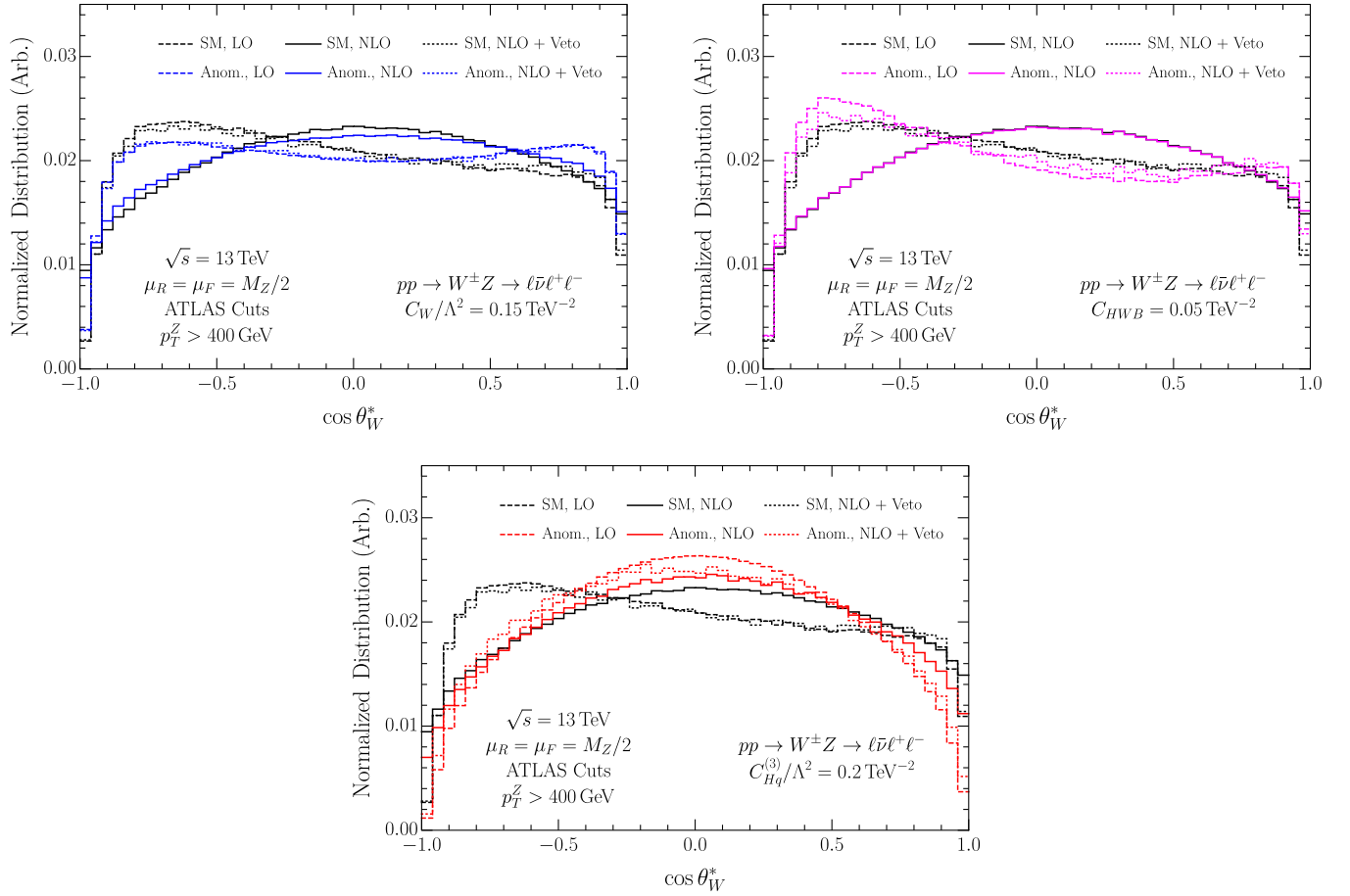
FIG. 2. Normalized distributions of the angular variable, $\cos\theta_W^*$ in WZ production at 13 TeV, requiring $p_T^Z > 400$ GeV. In each figure we show the SM curve (black) for comparison along with an anomalous-coupling point: $C_W/\Lambda^2 = 0.15$ TeV^{-2} (upper left), $C_{HWB}/\Lambda^2 = 0.05$ TeV^{-2} (upper right), and $C_{Hq}^{(3)}/\Lambda^2 = 0.2$ TeV^{-2} (bottom). The points are chosen to be near the edge of the allowed regions by our combined fits to WV and VH production ($V = W^\pm, Z$). For each parameter point, we plot the distribution at LO (dashed lines), NLO (solid lines), and at NLO with a jet veto (dotted lines). The jet veto curves correspond to a veto on jets with $p_T^j > 150$ GeV. The figures are computed to $\mathcal{O}(1/\Lambda^4)$.

positively-charged lepton from the Z decay playing the role of the charged lepton in the W frame.

These angular variables are useful because their distributions are sensitive to the gauge boson polarizations [77]. They are of particular interest to us here because of the relationship between the longitudinally polarized vector bosons and the Higgs boson. Understanding the polarization fractions for high-energy vector bosons has been shown to be a useful probe for anomalous-coupling measurements at the LHC [60,77,81,82]. However, in Refs. [12,53] it was found that the sensitivity of $\cos\theta_W^*$ to the anomalous couplings was lost in the presence of an extra jet. This is a manifestation of QCD corrections breaking the noninterference between helicity amplitudes of the SM and the dimension-six SMEFT amplitudes, as originally pointed out in Ref. [83], and studied in the context of electroweak interactions in Ref. [84]. Here, we

consider the impact of vetoing hard jets on restoring the sensitivity of these distributions at NLO.

In Fig. 2, we present the normalized $\cos\theta_W^*$ distributions from $W^\pm Z$ production at LO, NLO, and at NLO with a 150 GeV jet veto. In all plots we also include a p_T^Z cut, $p_T^Z > 400$ GeV, in order to enhance our sensitivity to the anomalous couplings. In each figure we show the results for the SM as well as with one of three anomalous couplings: $C_W/\Lambda^2 = 0.15$ TeV^{-2} (upper left), $C_{HWB}/\Lambda^2 = 0.05$ TeV^{-2} (upper right), and $C_{Hq}^{(3)}/\Lambda^2 = 0.2$ TeV^{-2} (bottom). As is clear from comparing the LO (dashed) and NLO (solid) curves, the hard radiation present in $W^\pm Z$ production at NLO washes out much of the sensitivity to anomalous couplings, as the SM and anomalous-coupling curves are essentially indistinguishable at NLO, despite the differences at LO. With a veto on hard jets, however, the sensitivity is restored, essentially to the levels obtained at LO.
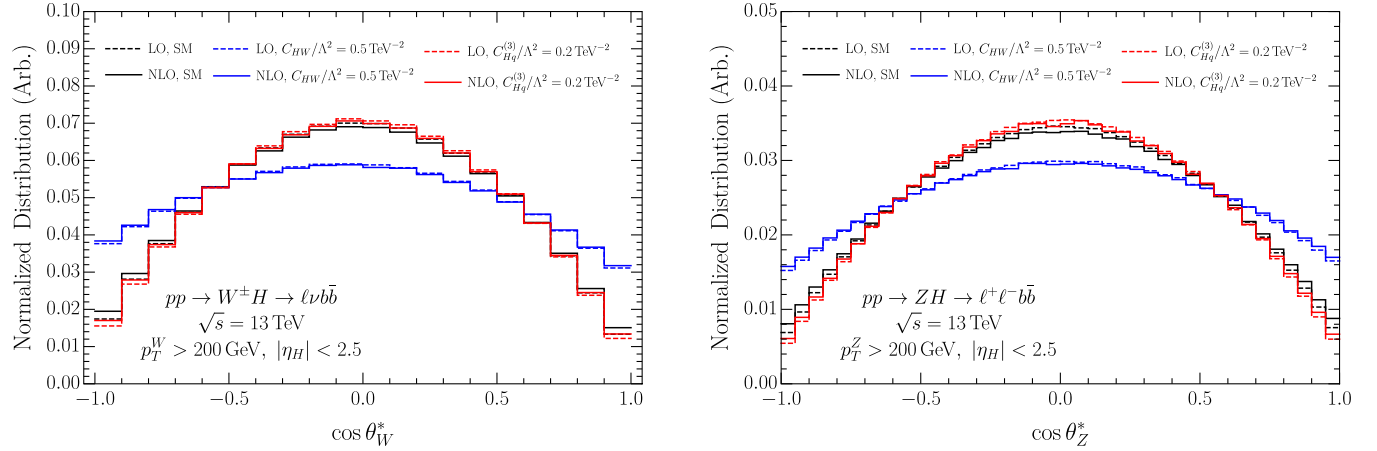
FIG. 3. Normalized distributions of the angular variable $\cos\theta_W^*$ in WH production (left) and $\cos\theta_Z^*$ in ZH production (right), both at 13 TeV and requiring the vector boson to have $p_T^V > 200$ GeV and the Higgs rapidity to lie within ± 2.5. In each figure, we present the results at LO (dashed lines) and NLO (solid lines) for three different parameter points: the SM (black lines), with $C_{HW}/\Lambda^2 = 0.5$ TeV^{-2} (blue lines), and with $C_{Hq}^{(3)}/\Lambda^2 = 0.2$ TeV^{-2} (red lines). The figures are computed to $\mathcal{O}(1/\Lambda^4)$.

At high energy, only the (00) polarization (where both gauge bosons are longitudinally polarized) and $(\pm, \mp)$ (transverse polarizations) survive [76], and the angular distributions of the polarizations are different. The longitudinal polarization amplitude receives no contribution from the anomalous gauge couplings in the high-energy limit. Furthermore, only C_W contributes to the high-energy limit of the $(\pm, \mp)$ amplitude. We also note that when only C_{HWB} is turned on (pink curves, upper right in Fig. 2), the anomalous couplings $\lambda^Z = \lambda^\gamma$ are fixed to zero. Here, we see that at $\cos\theta_W^* \sim -0.5$, the distribution is sensitive to the effects of a comparatively small value of C_{HWB} at LO, and this sensitivity is restored at NLO with the jet veto.

In Fig. 3, we show the normalized distributions of the analogous angular variables but for $W^\pm H$ and ZH production. We plot the results at LO (dashed lines) and NLO (solid lines) for $C_{HW}/\Lambda^2 = 0.5$ TeV^{-2} (blue lines) and $C_{Hq}^{(3)}/\Lambda^2 = 0.2$ TeV^{-2} (red lines). Here, we see that with $C_{Hq}^{(3)}$ nonzero, the distribution has a very similar shape to the SM piece, as both are dominated by the longitudinally polarized helicity amplitudes at high p_T. The distribution with nonzero C_{HW}, however, enhances the transverse parts of the amplitude, and thus has a shape that is enhanced at $\cos\theta_V^* = \pm 1$. This can be clearly seen in the LO results of Ref. [78]. In contrast to $W^\pm Z$, these distributions are largely unchanged by the higher-order corrections, and they maintain their sensitivity to anomalous couplings that enhance the transverse polarizations even in the presence of radiation.

D. Sensitivity to anomalous couplings

We can also consider how the jet veto changes the sensitivity to anomalous couplings in other $W^\pm Z$ distributions. If we decompose a generic differential cross section up to $\mathcal{O}(\Lambda^{-4})$ as

$$\sigma(C_i) = \sigma_{\text{SM}} + \Delta\sigma_{\Lambda^2}(C_i) + \Delta\sigma_{\Lambda^4}(C_i^2), \qquad (12)$$

we can isolate parts of the cross section that depend linearly and quadratically on the Wilson coefficients, and see how these parts grow with energy at LO, and in the presence of radiation. (The quadratic terms include the contributions depending on two different coefficients.) This is done in Fig. 4 for $W^\pm Z$ production with $C_W/\Lambda^2 = 0.15$ TeV^{-2} (top) and $C_{Hq}^{(3)}/\Lambda^2 = 0.2$ TeV^{-2} (bottom) in bins of $m_{T,WZ}$ for the Λ^{-2} (left) and Λ^{-4} (right) pieces, respectively.

We see immediately that the presence of QCD radiation makes a substantial difference in the sensitivity of the distributions to anomalous couplings. Focusing first on the linear pieces, we note that these arise from the interference between the dimension-six SMEFT part of the amplitude with the SM part, and are thus subject to the noninterference effects noted in Refs. [60,77,81]. At high energies, the SM amplitude receives contributions from both longitudinally and oppositely polarized transverse gauge bosons. The portion of the amplitude proportional to C_W, however, has only transverse polarizations. The resulting noninterference between the SM and the dimension-six SMEFT amplitudes is clear from the blue curve in Fig. 4 (upper left), which does not substantially grow with energy. As discussed in Ref. [84],[2] however, the presence of an extra quark or gluon in the matrix element allows for this interference to be restored, and indeed, we see that the interference term at NLO (with or without a jet veto) grows substantially at high m_T^{WZ}. That this enhanced sensitivity to the interference persists even with a veto on the hard jets arising from the real emission implies that the virtual

---

[2]This was originally pointed out in a slightly different context in Ref. [83].
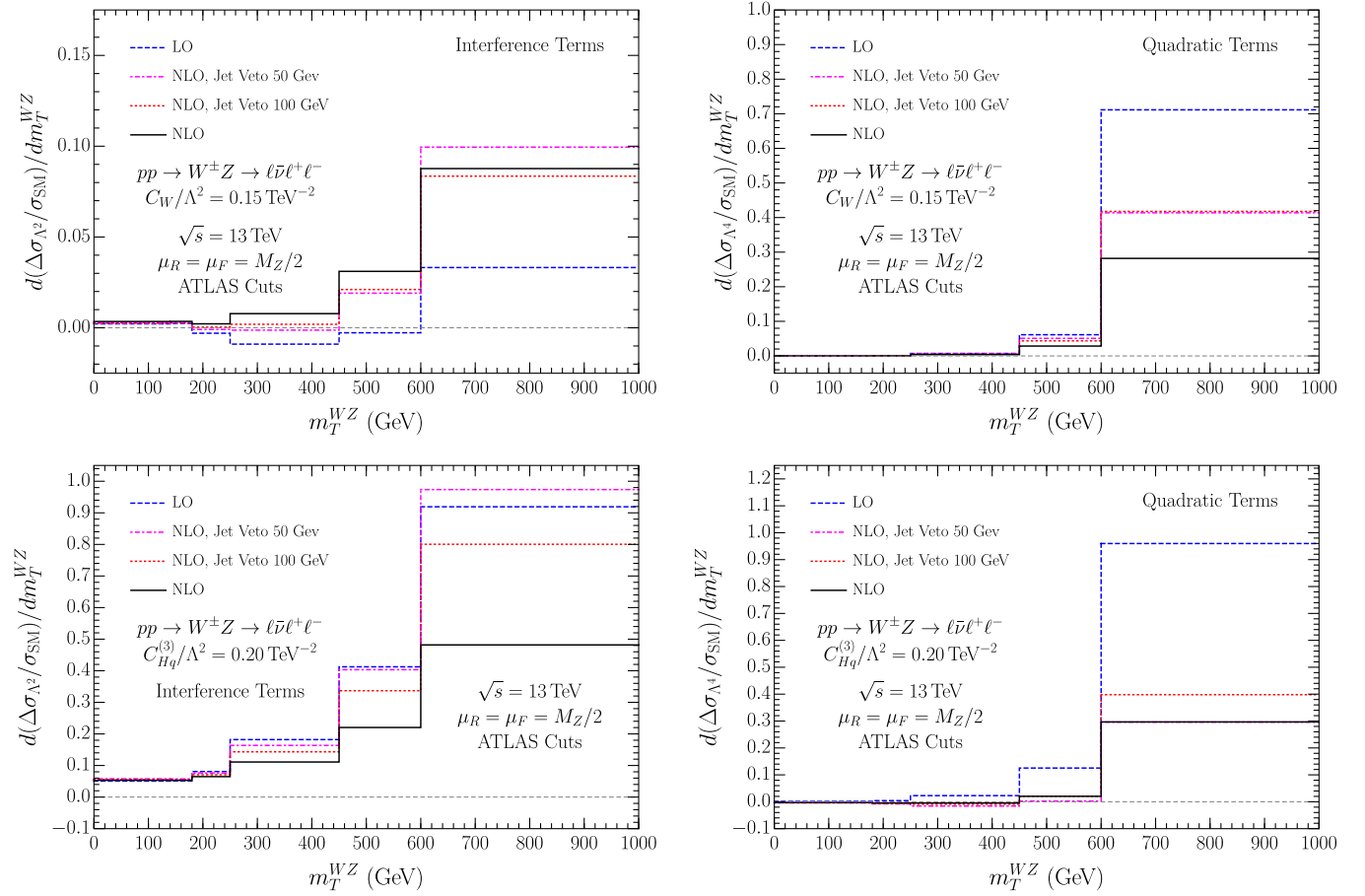
FIG. 4. The sensitivity of the m_T^{WZ} distributions to anomalous gauge (top) and fermion (bottom) couplings, at LO and NLO with varying jet vetos. See text for details.

corrections play an important role in restoring the interference.

For the interference term proportional to $C_{Hq}^{(3)}$, the story is somewhat different. Here, we see that there is a growth in sensitivity at high energies even at LO, as the $C_{HQ}^{(3)}$ amplitude enhances the longitudinal parts of the amplitude which are already dominant in the SM part at high energies. At NLO, much of this sensitivity is washed out due to the presence of hard jets, but a great deal of the sensitivity can be restored by imposing a veto on the hard real emission.

Turning now to the $\mathcal{O}(\Lambda^{-4})$ terms, we see immediately on the right-hand side of Fig. 4 that the LO distributions exhibit much faster growth with energy than the corresponding NLO curves, for both C_W and $C_{Hq}^{(3)}$. The $\mathcal{O}(\Lambda^{-4})$ terms do not depend on any interference with the SM amplitude, so the sensitivity is dictated largely by the kinematics of the process. For anomalous gauge couplings, this was studied in Ref. [53], where it was found that $W^{\pm}Z$ production at NLO generically allows for hard jets, which suppresses the sensitivity to the anomalous-coupling pieces [which grow like $(\text{Energy})^2$]. It was found there that much of the sensitivity in this distribution can be regained by

veting events containing hard jets. The same conclusion is apparent for both C_W and $C_{Hq}^{(3)}$ in Fig. 2, where vetoing jets with $p_T > 150$ GeV restores much of the sensitivity obtained at LO.

In principle, one could perform the same analysis on the $\mathcal{O}(\Lambda^{-2})$ and $\mathcal{O}(\Lambda^{-4})$ terms in the $W^{\pm}H$ distributions. In practice, though, the results are significantly less interesting when comparing LO to NLO. This is because, as shown in Ref. [53], the real emission contributions to $W^{\pm}H$ production at NLO are typically soft, in contrast to the hard jets that appear in $W^{\pm}Z$ production. Thus, a veto on hard jets in $W^{\pm}H$ production at NLO does not significantly change the sensitivity to anomalous couplings, at either $\mathcal{O}(\Lambda^{-2})$ or $\mathcal{O}(\Lambda^{-4})$. Furthermore, as can be seen in Fig. 1, the K factors are only mildly dependent on the anomalous couplings, so the sensitivity at LO and NLO to all higher-dimension operators is largely the same.

IV. FITS TO WARSAW COEFFICIENTS

A. Datasets and fitting procedure

Section III B demonstrates that the implementation of NLO QCD within the SMEFT can have a significant

TABLE IV. Experimental data included in our study. The third column shows the number of bins used in our analysis, always counting from the highest. Int. lum. stands for the integrated luminosity.

Channel	Distribution	Number of bins	Dataset	Int. lum.
$W^\pm H \to b\bar{b}\ell^\pm + \not{E}_T$	p_T^W, Fig. 3	2	ATLAS 8 TeV	79.8 fb^{-1} [85]
$ZH \to b\bar{b}\ell^+\ell^-$ or $b\bar{b} + \not{E}_T$	p_T^Z, Fig. 3	3	ATLAS 8 TeV	79.8 fb^{-1} [85]
$W^+W^- \to \ell^+\ell'^- + \not{E}_T(0j)$	$p_T^{\text{leading,lepton}}$, Fig. 11	1	ATLAS 8 TeV	20.3 fb^{-1} [86]
$W^+W^- \to e^\pm\mu^\mp + \not{E}_T(0j)$	$p_T^{\text{leading,lepton}}$, Fig. 7	5	ATLAS 13 TeV	36.1 fb^{-1} [87]
$W^\pm Z \to \ell^+\ell^-\ell^{(\prime)\pm}$	m_T^{WZ}, Fig. 5	2	ATLAS 8 TeV	20.3 fb^{-1} [88]
$W^\pm Z \to \ell^+\ell^-\ell^{(\prime)\pm} + \not{E}_T$	Z candidate $p_T^{\ell\ell}$, Fig. 5	9	CMS 8 TeV	19.6 fb^{-1} [89]
$W^\pm Z \to \ell^+\ell^-\ell^{(\prime)\pm}$	m_T^{WZ}, Fig. 4(c)	6	ATLAS 13 TeV	36.1 fb^{-1} [79]
$W^\pm Z \to \ell^+\ell^-\ell^{(\prime)\pm} + \not{E}_T$	m^{WZ}, Fig. 15(a)	3	CMS 13 TeV,	35.9 fb^{-1} [90]

impact on distributions. These changes lead to different predictions from those obtained by using LO QCD in the SMEFT with the appropriate Standard Model K factor. We further solidify the need to include NLO QCD within SMEFT fits by showing the differences between fits with and without NLO. We also show that including $\mathcal{O}(1/\Lambda^4)$ can significantly improve the fits. Lastly, the $\mathcal{O}(1/\Lambda^4)$ terms allow one to explore if the values of coefficients are consistent with a weakly- or strongly-coupled theory.

We fit to the ten Warsaw basis coefficients described in Sec. II at both LO and NLO in the SMEFT to quantify these effects. We calculate uncorrelated χ^2 fits to differential cross section measurements for the processes $W^\pm H, ZH,$ $W^+W^-,$ and $W^\pm Z$ and we construct the χ^2 function for a given anomalous-coupling input, $\vec{C}$, as

$$\chi^2(\vec{C}) = \sum_{\substack{\text{processes} \\ WH,ZH \\ WW,WZ}} \sum_\alpha^{\text{datasets}} \sum_i^{\text{bins}} \frac{(\epsilon_{i\alpha}\hat{O}(\vec{C})_{i\alpha}^{\text{theory}} - \hat{O}_{i\alpha}^{\text{exp}})^2}{(v_{i\alpha}^{\text{exp}})^2}, \quad (13)$$

where $\hat{O}(\vec{C})_{i\alpha}^{\text{theory}}$, $\hat{O}_{i\alpha}^{\text{exp}}$, and $v_{i\alpha}^{\text{exp}}$ are, respectively, the theoretical expected value, experimental observation, and estimated uncertainties for the ith bin of dataset α. An efficiency factor, $\epsilon_{i\alpha}$, is introduced to account for an overall scaling of the simulation data, where $\epsilon_{i\alpha}$ is calculated by taking the ratio of the experimentally simulated value for the SM differential cross section over our prediction for the differential cross section with an SM input ($\vec{C} = 0$) for the ith bin of dataset α.

The datasets that go into each process are detailed in Table IV. The uncertainties are estimated by combining reported statistical and systemic uncertainties in quadrature, assuming an overall 5% systematic uncertainty bin by bin, neglecting correlations.

We explore two methods for calculating confidence intervals of the Warsaw coefficients: projecting all but one coefficient to zero and alternatively profiling over the remaining coefficients to minimize the χ^2 function at each point. The numerical results obtained by fitting

TABLE V. The 95% confidence interval fits to individual EFT coefficients using $W^+W^- + W^\pm Z + ZH + W^\pm H$ data, with Λ fixed to 1 TeV.

	$W^+W^- + W^\pm Z + ZH + W^\pm H$ projected				$W^+W^- + W^\pm Z + ZH + W^\pm H$ profiled			
	Λ^{-4}		Λ^{-2}		Λ^{-4}		Λ^{-2}	
	LO	NLO	LO	NLO	LO	NLO	LO	NLO
C_{HWB}	$(-0.05, 0.03)$	$(-0.09, 0.04)$	$(-0.07, 0.02)$	$(-0.14, 0.03)$	$(-0.70, 0.47)$	$(-0.75, 0.50)$	$(-2.9, 2.3)$	$(-4.4, 1.5)$
$C_{Hq}^{(3)}$	$(-0.02, 0.08)$	$(-0.02, 0.11)$	$(-0.02, 0.09)$	$(-0.02, 0.14)$	$(-0.26, 0.62)$	$(-0.30, 0.67)$	$(-0.17, 0.82)$	$(-0.38, 0.82)$
C_{HD}	$(-0.12, 0.06)$	$(-0.21, 0.08)$	$(-0.15, 0.05)$	$(-0.30, 0.07)$	$(-1.1, 2.1)$	$(-1.2, 2.4)$	$(-4.5, 6.8)$	$(-2.6, 9.1)$
$C_{Hq}^{(1)}$	$(-0.16, 0.21)$	$(-0.18, 0.19)$	$(-0.24, 0.20)$	$(-0.32, 0.15)$	$(-0.21, 0.38)$	$(-0.25, 0.40)$	$(-0.45, 0.93)$	$(-0.81, 0.71)$
C_{Hu}	$(-0.30, 0.22)$	$(-0.33, 0.24)$	$(-0.34, 0.72)$	$(-0.38, 0.81)$	$(-0.43, 0.59)$	$(-0.46, 0.62)$	$(-23.0, 23.0)$	$(-42.0, 48.0)$
C_{HW}	$(-1.1, 0.55)$	$(-1.2, 0.56)$	$(-0.52, 0.92)$	$(-0.52, 0.92)$	$(-1.4, 2.4)$	$(-1.5, 0.51)$	$(-31.0, 19.0)$	$(-33.0, 17.0)$
C_W	$(-0.13, 0.13)$	$(-0.20, 0.18)$	$(-1.4, 1.3)$	$(-0.28, 0.93)$	$(-0.14, 0.14)$	$(-0.20, 0.19)$	$(-1.3, 1.9)$	$(-3.2, 2.1)$
C_{Hd}	$(-0.31, 0.35)$	$(-0.33, 0.38)$	$(-2.2, 1.1)$	$(-2.2, 1.0)$	$(-0.62, 0.45)$	$(-0.67, 0.48)$	$(-82.0, 86.0)$	$(-13.0, 14.0)$
$C_{H\Box}$	$(-4.9, 6.3)$	$(-4.9, 6.3)$	$(-4.6, 8.6)$	$(-4.6, 8.6)$	$(-57.0, 20.0)$	$(-59.0, 20.0)$	$(-27.0, 43.0)$	$(-25.0, 43.0)$
C_{HB}	$(-2.8, 2.3)$	$(-2.9, 2.4)$	$(-6.1, 11.0)$	$(-6.0, 12.0)$	$(-3.1, 3.8)$	$(-3.3, 4.0)$	$(-31.0, 22.0)$	$(-31.0, 21.0)$
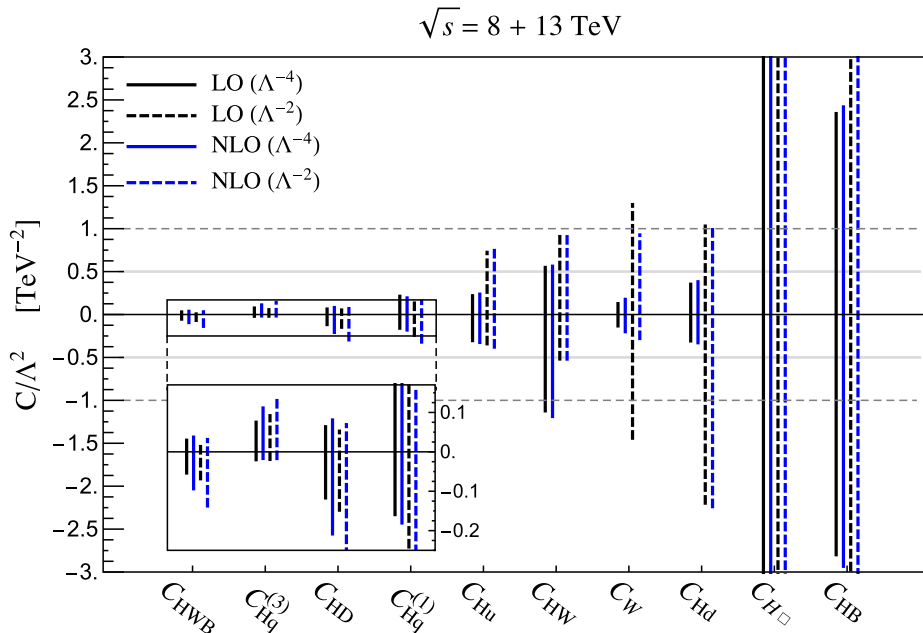
FIG. 5. The 95% confidence interval fits to individual EFT coefficients using $W^+W^- + W^\pm Z + ZH + W^\pm H$ data. All other SMEFT coefficients are projected to zero. Fits quadratic in $1/\Lambda^2$ (linear) LO and NLO QCD are shown as solid (dashed) black and blue lines, respectively.

all[3] processes using both profiling and projecting are given in Table V. They are compared graphically in Figs. 5 and 6. Overall we see that the projected limits are significantly more stringent than the profiled. This is to be expected since the profiling allows for more flexibility in the χ^2 function. The profiling method demonstrates the multidimensional nature of the fit.

We also show several two-dimensional (2D) confidence interval fits using the projection method in Fig. 7. In principle one could make a 2D confidence interval for each combination of Warsaw coefficients. However, most of these plots end up with similar results, showing order 20% NLO effects and with many of the regions falling in the strongly-coupled regime. We have selected some example plots that are particularly demonstrative and also correspond to interesting electroweak precision variables (S and T).

B. Importance of NLO QCD and quadratic order fits

The 95% confidence intervals for the projected individual parameters are shown in Fig. 5. We have included solid (dashed) grey lines at ± 0.5 (1.0) to guide the eye. Similarly, we show the individual 95% confidence intervals from the profiled fitting procedure in Fig. 6. The solid (dashed) lines are now at ± 2.0 (4.0) and the scales have been expanded. Black (blue) lines indicate that we are working to LO

(NLO) QCD in the SMEFT, and solid (dashed) lines indicate the expansion to $\mathcal{O}(\frac{1}{\Lambda^4})$ [$\mathcal{O}(\frac{1}{\Lambda^2})$].

Similarly, we show the 95% confidence intervals for some selected planes of parameters using the projected method in Fig. 7 for LO (inside black curve) and NLO (inside blue curve) QCD in the SMEFT, along with the limits from electroweak precision observables (EWPO) [91] (inside red curve) to $\mathcal{O}(\frac{1}{\Lambda^4})$, using the χ^2 fit of Ref. [92].[4] Again, we emphasize that our results are not meant to compete with the global fits including Higgs data and EWPO, but rather, our goal is to determine the importance of NLO QCD within the SMEFT and to examine the $1/\Lambda^2$ dependence. The EWPO curves are included, however, as a reference for comparison.

First, let us compare the differences of the LO and NLO QCD fits in the SMEFT, the black and blue lines. Looking at the results in Figs. 5 and 6, including NLO QCD in the SMEFT can change the fit intervals on the order of 10%–20%, on average. For some coefficients, NLO QCD can have an effect as large as 50%. From the two-dimensional plots in Fig. 7, we see that going from LO to NLO QCD can shift the curves by as much as 25% in some directions, along with altering the overall orientation and shapes of the curves.

Next we compare the differences in the fits when working to $\mathcal{O}(\frac{1}{\Lambda^4})$ versus $\mathcal{O}(\frac{1}{\Lambda^2})$, the solid and dashed lines. The $\mathcal{O}(\frac{1}{\Lambda^4})$ fits are always better or comparable to the $\mathcal{O}(\frac{1}{\Lambda^2})$

---

[3]The fits to individual processes can by compared in Tables VI, VII, and VIII located in Appendix.

[4]Reference [92] demonstrates in the case of the EWPO the important effects from including both QCD and electroweak SMEFT NLO corrections.
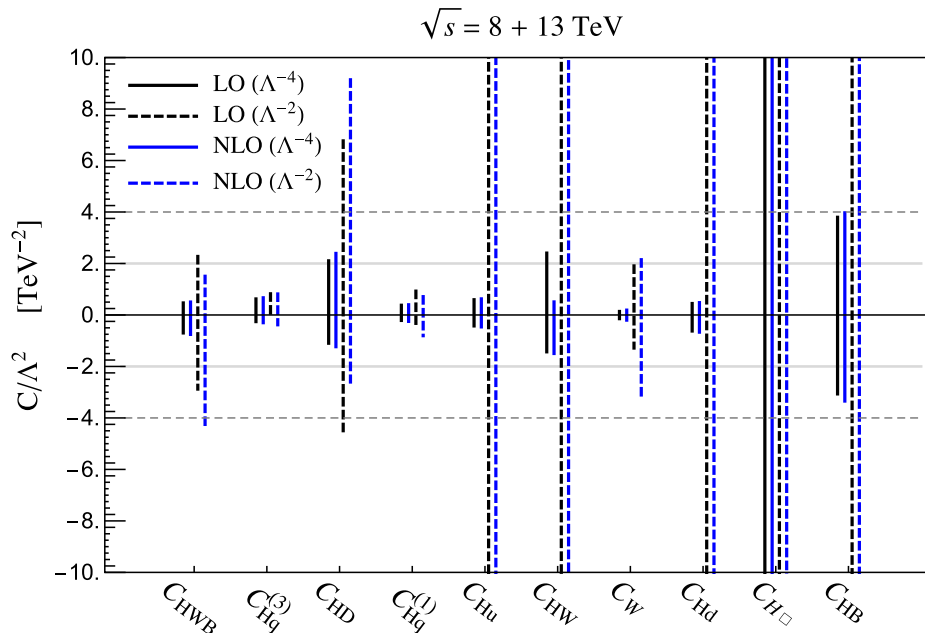
FIG. 6. The 95% confidence interval fits to individual EFT coefficients using $W^+W^- + W^\pm Z + ZH + W^\pm H$ data and profiling over all other coefficients. Fits quadratic in $1/\Lambda^2$ (linear) LO and NLO QCD are shown as solid (dashed) black and blue lines, respectively.

fits. On average, working to $\mathcal{O}(\frac{1}{\Lambda^4})$ improves the fits by a factor of 2 and as much as a factor of 10 in some of the profiled fits. Such a large improvement in the fit hints that the coefficients no longer correspond to a weakly-coupled theory, and we discuss this in more detail in the following section. Similar results when comparing the $\mathcal{O}(\frac{1}{\Lambda^4})$ fits to those obtained at $\mathcal{O}(\frac{1}{\Lambda^2})$ were obtained in Ref. [1] at LO QCD.

C. The validity of weakly-coupled theory

We decompose the differential cross sections as in Eq. (12). The SMEFT couplings generically scale as $\alpha_{\mathrm{EFT}} \sim \frac{g_{\mathrm{EFT}}^2 v^2}{\Lambda^2}$ or $\frac{g_{\mathrm{EFT}}^2 \mathrm{Energy}^2}{\Lambda^2}$, where g_{EFT} parametrizes the strength of the underlying UV complete theory. The linear piece, $\Delta\sigma_{\Lambda^2}$, goes as $\mathcal{O}(\alpha_{\mathrm{EFT}})$, and the quadratic piece $\Delta\sigma_{\Lambda^4}$ goes as $\mathcal{O}(\alpha_{\mathrm{EFT}}^2)$. In a weakly-coupled theory, one generically expects $\alpha_{\mathrm{EFT}} \lesssim 1$. This implies $\Delta\sigma_{\Lambda^4}/\Delta\sigma_{\Lambda^2} \lesssim 1$ for a weakly-coupled theory, assuming that there are no cancellations in the underlying UV theory. Alternatively, one might also consider the upper limit on a weakly-coupled theory to be $\alpha_{\mathrm{EFT}} \lesssim 4\pi$ as some sort of perturbative unitarity bound. Similar criteria have been explored elsewhere in the literature [7,56].

In Fig. 7, we show different regions detailing the strength of the coupling by comparing the differential cross sections in each bin. All parameters not shown in the plot are projected to zero. The white regions in the figures indicate that $\Delta\sigma_{\Lambda^4}/\Delta\sigma_{\Lambda^2} < 1$ for all bins in all of the processes considered. One may consider this the weakly-coupled regime. The grey and blue regions, respectively, indicate

that $\Delta\sigma_{\Lambda^4}/\Delta\sigma_{\Lambda^2} > 1$ and $\Delta\sigma_{\Lambda^4}/\Delta\sigma_{\Lambda^2} > 4\pi$ in at least one bin for at least one process. Any coefficient or fit in these regions would no longer be considered part of a weakly-coupled theory.

We see in Fig. 7 that many of the confidence intervals we derived for the $WV + VH$ data (within the blue or black curves) fall within a grey shaded region. If the coefficients lie in this area, they correspond to a strongly-interacting theory and higher-dimension operators need to be retained. In contrast, the bounds from the EWPO (within the red curves) place strong constraints on the couplings and typically fall within the weakly-coupled regime (white region). One might consider setting an experimental goal of LHC to have all fits sufficiently precise such that they could probe the weakly-coupled regime. In this way one could fully understand the fits in terms of dimension-six operators.

There are small regions protruding into some of the regions within the plots. They are particularly evident in the top left plot in Fig. 7. These can be seen in other plots not displayed here. They can be understood as cancellations within the helicity amplitudes.

We also note that as Warsaw coefficients are increased, the last bin will be the first indication that the weakly-coupled theory is no longer valid. The argument is similar to those made in previous works showing that most of the fitting power comes from the last bin [78]. We know SM cross sections are falling with increasing energy, while the quadratic SMEFT piece grows with energy. Therefore the bin with the largest energy, the last one, will have the largest deviation from the SM and the best fitting power.
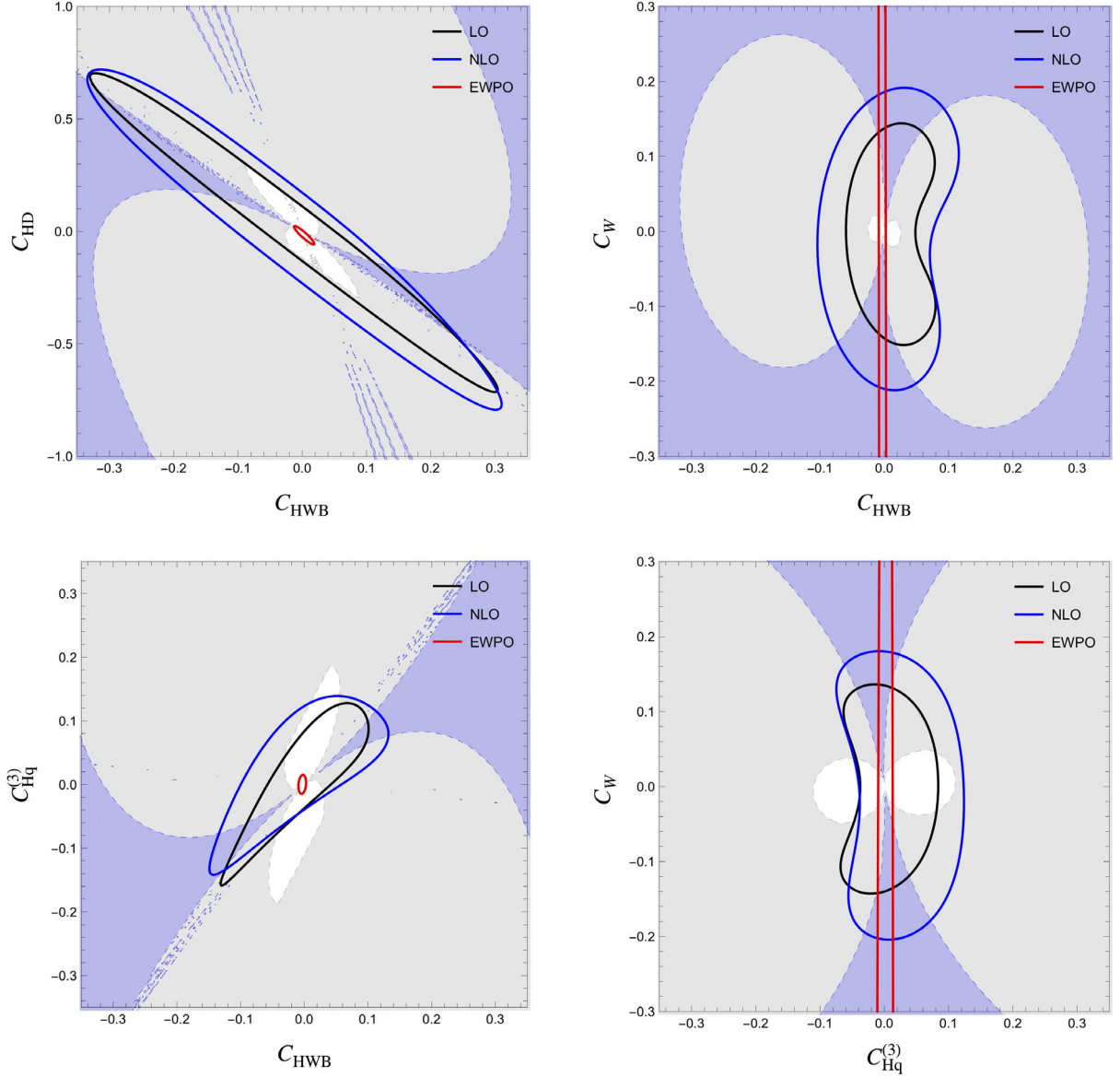
FIG. 7. The 95% confidence region in the $C_{HWB} - C_{HD}$ (top left), $C_{HWB} - C_W$ (top right), $C_{HWB} - C_{Hq}^{(3)}$ (bottom left), and $C_{Hq}^{(3)} - C_W$ (bottom right) planes with all other EFT coefficients projected to zero and Λ fixed to 1 TeV. Quadratic fits to $W^+W^- + W^\pm Z + ZH + W^\pm H$ distributions are shown in black (blue) for LO (NLO) QCD in SMEFT, while the quadratic fit to NLO electroweak precision observables is shown in red. The grey (blue) region indicates the coefficients no longer correspond to a weakly coupled theory that is $\Delta\sigma_{\Lambda^4} > \Delta\sigma_{\Lambda^2}(4\pi\Delta\sigma_{\Lambda^2})$.

V. CONCLUSION

As the quest for discovering beyond-Standard-Model particles continues without any direct observations, it is important to understand all the data we have to the best precision. Such precision measurements could be the first evidence for some new high-scale physics. To this end, we have studied the effects of NLO QCD in the SMEFT on the $W^+W^-, W^\pm Z, W^\pm H$, and ZH production at the LHC. We find that including QCD radiation can have a significant effect on the parameters. This implies that global SMEFT fits including Higgs data and EWPO need to be done beyond LO

in QCD. We have also explored the numerical differences between the $1/\Lambda^2$ and $1/\Lambda^4$ fits. Their differences suggest that current fits to LHC data are not yet sensitive to weakly-coupled theories for the majority of coefficients.

Primitive cross sections at 8 and 13 TeV for $W^\pm Z$ production with jet vetoes and at 13 TeV for $W^\pm H$ production are posted at [93].

ACKNOWLEDGMENTS

APPENDIX: NUMERICAL FITS

We show tables detailing the numerical results of the 95% confidence intervals to different subsets of processes in Tables VI, VII, and VIII. Entries with a "$\cdots$" mean no fit was performed, since the process does not depend on that parameter. Overall, fitting to a few bins in $W^{\pm}H$ and ZH processes yields comparable sensitivity to that of the W^+W^- and $W^{\pm}Z$ fits for some parameters.

TABLE VI.   The 95% confidence interval fits to individual EFT coefficients using $W^{\pm}H$ and ZH data, with Λ fixed to 1 TeV.

| | $W^{\pm}H$ projected | | | | ZH projected | | | |
| | Λ^{-4} | | Λ^{-2} | | Λ^{-4} | | Λ^{-2} | |
	LO	NLO	LO	NLO	LO	NLO	LO	NLO
C_{HWB}	$\cdots$	$\cdots$	$\cdots$	$\cdots$	$(-3.1, 1.8)$	$(-3.3, 1.8)$	$(-1.8, 3.4)$	$(-1.8, 3.4)$
$C_{Hq}^{(3)}$	$(-0.61, 0.19)$	$(-0.65, 0.20)$	$(-0.20, 0.26)$	$(-0.22, 0.29)$	$(-0.33, 0.12)$	$(-0.35, 0.13)$	$(-0.08, 0.18)$	$(-0.09, 0.20)$
C_{HD}	$(-33.0, 16.0)$	$(-33.0, 16.0)$	$(-63.0, 53.0)$	$(-63.0, 53.0)$	$(-17.0, 21.0)$	$(-17.0, 21.0)$	$(-14.0, 26.0)$	$(-14.0, 26.0)$
$C_{Hq}^{(1)}$	$\cdots$	$\cdots$	$\cdots$	$\cdots$	$(-0.20, 0.22)$	$(-0.21, 0.24)$	$(-1.9, 0.77)$	$(-2.0, 0.82)$
C_{Hu}	$\cdots$	$\cdots$	$\cdots$	$\cdots$	$(-0.31, 0.22)$	$(-0.34, 0.24)$	$(-0.33, 0.76)$	$(-0.37, 0.85)$
C_{HW}	$(-1.2, 0.59)$	$(-1.2, 0.61)$	$(-0.96, 1.1)$	$(-0.96, 1.1)$	$(-1.5, 0.75)$	$(-1.5, 0.77)$	$(-0.69, 1.3)$	$(-0.69, 1.3)$
C_W	$\cdots$	$\cdots$	$\cdots$	$\cdots$	$\cdots$	$\cdots$	$\cdots$	$\cdots$
C_{Hd}	$\cdots$	$\cdots$	$\cdots$	$\cdots$	$(-0.31, 0.36)$	$(-0.34, 0.39)$	$(-2.3, 1.0)$	$(-2.3, 1.0)$
$C_{H\square}$	$(-41.0, 8.2)$	$(-41.0, 8.2)$	$(-13.0, 16.0)$	$(-13.0, 16.0)$	$(-6.5, 7.8)$	$(-6.5, 7.8)$	$(-5.2, 9.7)$	$(-5.2, 9.7)$
C_{HB}	$\cdots$	$\cdots$	$\cdots$	$\cdots$	$(-2.8, 2.3)$	$(-2.9, 2.4)$	$(-6.1, 11.0)$	$(-6.0, 12.0)$

TABLE VII.   The same as Table VI, but using W^+W^- and $W^{\pm}Z$ data, with Λ fixed to 1 TeV.

| | W^+W^- projected | | | | $W^{\pm}Z$ projected | | | |
| | Λ^{-4} | | Λ^{-2} | | Λ^{-4} | | Λ^{-2} | |
	LO	NLO	LO	NLO	LO	NLO	LO	NLO
C_{HWB}	$(-0.14, 0.17)$	$(-0.14, 0.18)$	$(-0.35, 0.38)$	$(-0.37, 0.4)$	$(-0.05, 0.03)$	$(-0.1, 0.03)$	$(-0.07, 0.02)$	$(-0.14, 0.03)$
$C_{Hq}^{(3)}$	$(-0.34, 0.21)$	$(-0.35, 0.22)$	$(-0.33, 0.3)$	$(-0.35, 0.32)$	$(-0.03, 0.08)$	$(-0.03, 0.15)$	$(-0.03, 0.1)$	$(-0.03, 0.18)$
C_{HD}	$(-0.35, 0.54)$	$(-0.36, 0.56)$	$(-0.60, 0.69)$	$(-0.64, 0.73)$	$(-0.12, 0.06)$	$(-0.22, 0.07)$	$(-0.15, 0.05)$	$(-0.32, 0.06)$
$C_{Hq}^{(1)}$	$(-0.37, 0.34)$	$(-0.38, 0.35)$	$(-4.8, 3.1)$	$(-5.4, 3.4)$	$(-0.26, 1.7)$	$(-1.5, 0.43)$	$(-0.15, 2.8)$	$(-1.3, 0.45)$
C_{Hu}	$(-0.47, 0.41)$	$(-0.48, 0.42)$	$(-3.1, 2.4)$	$(-3.4, 2.6)$	$\cdots$	$\cdots$	$\cdots$	$\cdots$
C_{HW}	$\cdots$	$\cdots$	$\cdots$	$\cdots$	$\cdots$	$\cdots$	$\cdots$	$\cdots$
C_W	$(-0.22, 0.23)$	$(-0.23, 0.23)$	$(-4.4, 5.1)$	$(-9.6, 6.8)$	$(-0.14, 0.13)$	$(-0.22, 0.19)$	$(-1.5, 1.3)$	$(-0.27, 0.94)$
C_{Hd}	$(-0.59, 0.62)$	$(-0.59, 0.63)$	$(-7.6, 9.7)$	$(-8.0, 10.0)$	$\cdots$	$\cdots$	$\cdots$	$\cdots$
$C_{H\square}$	$\cdots$	$\cdots$	$\cdots$	$\cdots$	$\cdots$	$\cdots$	$\cdots$	$\cdots$
C_{HB}	$\cdots$	$\cdots$	$\cdots$	$\cdots$	$\cdots$	$\cdots$	$\cdots$	$\cdots$

TABLE VIII.   The same as Table VI, but using $ZH + W^{\pm}H$ and $W^+W^- + W^{\pm}Z$ data, with Λ fixed to 1 TeV.

| | $ZH + W^{\pm}H$ projected | | | | $W^+W^- + W^{\pm}Z$ projected | | | |
| | Λ^{-4} | | Λ^{-2} | | Λ^{-4} | | Λ^{-2} | |
	LO	NLO	LO	NLO	LO	NLO	LO	NLO
C_{HWB}	$(-3.1, 1.8)$	$(-3.3, 1.8)$	$(-1.8, 3.4)$	$(-1.8, 3.4)$	$(-0.05, 0.03)$	$(-0.09, 0.04)$	$(-0.07, 0.02)$	$(-0.14, 0.03)$
$C_{Hq}^{(3)}$	$(-0.32, 0.12)$	$(-0.34, 0.13)$	$(-0.07, 0.16)$	$(-0.07, 0.18)$	$(-0.03, 0.08)$	$(-0.03, 0.14)$	$(-0.03, 0.10)$	$(-0.03, 0.17)$
C_{HD}	$(-16.0, 19.0)$	$(-16.0, 19.0)$	$(-14.0, 24.0)$	$(-14.0, 24.0)$	$(-0.12, 0.06)$	$(-0.21, 0.08)$	$(-0.15, 0.05)$	$(-0.30, 0.07)$
$C_{Hq}^{(1)}$	$(-0.17, 0.21)$	$(-0.18, 0.23)$	$(-0.27, 0.18)$	$(-0.30, 0.20)$	$(-0.31, 0.37)$	$(-0.40, 0.28)$	$(-0.33, 2.5)$	$(-1.3, 0.41)$
C_{Hu}	$(-0.31, 0.22)$	$(-0.34, 0.24)$	$(-0.33, 0.76)$	$(-0.37, 0.85)$	$(-0.47, 0.41)$	$(-0.48, 0.42)$	$(-3.1, 2.4)$	$(-3.4, 2.6)$
C_{HW}	$(-1.1, 0.55)$	$(-1.2, 0.56)$	$(-0.52, 0.92)$	$(-0.52, 0.92)$	$\cdots$	$\cdots$	$\cdots$	$\cdots$
C_W	$\cdots$	$\cdots$	$\cdots$	$\cdots$	$(-0.13, 0.13)$	$(-0.20, 0.18)$	$(-1.4, 1.3)$	$(-0.28, 0.93)$
C_{Hd}	$(-0.31, 0.36)$	$(-0.34, 0.39)$	$(-2.3, 1.0)$	$(-2.3, 1.0)$	$(-0.59, 0.62)$	$(-0.59, 0.63)$	$(-7.6, 9.7)$	$(-8.0, 10.0)$
$C_{H\square}$	$(-4.9, 6.3)$	$(-4.9, 6.3)$	$(-4.6, 8.6)$	$(-4.6, 8.6)$	$\cdots$	$\cdots$	$\cdots$	$\cdots$
C_{HB}	$(-2.8, 2.3)$	$(-2.9, 2.4)$	$(-6.1, 11.0)$	$(-6.0, 12.0)$	$\cdots$	$\cdots$	$\cdots$	$\cdots$

[1] E. da Silva Almeida, A. Alves, N. Rosa Agostinho, O. J. P. Éboli, and M. C. Gonzalez-Garcia, Electroweak sector under scrutiny: A combined analysis of LHC and electroweak precision data, Phys. Rev. D **99**, 033001 (2019).

[2] A. Biekotter, T. Corbett, and T. Plehn, The Gauge-Higgs legacy of the LHC Run II, SciPost Phys. **6**, 064 (2019).

[3] C. Grojean, M. Montull, and M. Riembau, Diboson at the LHC vs LEP, J. High Energy Phys. 03 (2019) 020.

[4] J. Ellis, C. W. Murphy, V. Sanz, and T. You, Updated global SMEFT fit to Higgs, Diboson and electroweak data, J. High Energy Phys. 06 (2018) 146.

[5] L. Berthier, M. Bjorn, and M. Trott, Incorporating doubly resonant $W^{\pm}$ data in a global fit of SMEFT parameters to lift flat directions, J. High Energy Phys. 09 (2016) 157.

[6] I. Brivio and M. Trott, The Standard Model as an effective field theory, Phys. Rep. **793**, 1 (2019).

[7] A. Falkowski, M. Gonzalez-Alonso, A. Greljo, D. Marzocca, and M. Son, Anomalous triple gauge couplings in the effective field theory approach at the LHC, J. High Energy Phys. 02 (2017) 115.

[8] W. Buchmuller and D. Wyler, Effective Lagrangian analysis of new interactions and flavor conservation, Nucl. Phys. **B268**, 621 (1986).

[9] B. Grzadkowski, M. Iskrzynski, M. Misiak, and J. Rosiek, Dimension-six terms in the Standard Model Lagrangian, J. High Energy Phys. 10 (2010) 085.

[10] J. Baglio, S. Dawson, and I. M. Lewis, An NLO QCD effective field theory analysis of W^+W^- production at the LHC including fermionic operators, Phys. Rev. D **96**, 073003 (2017).

[11] J. Baglio, S. Dawson, and I. M. Lewis, NLO effects in EFT fits to W^+W^- production at the LHC, Phys. Rev. D **99**, 035029 (2019).

[12] J. Baglio, S. Dawson, and S. Homiller, QCD corrections in Standard Model EFT fits to WZ and WW production, Phys. Rev. D **100**, 113010 (2019).

[13] S. Alioli, W. Dekens, M. Girard, and E. Mereghetti, NLO QCD corrections to SM-EFT dilepton and electroweak Higgs boson production, matched to parton shower in POWHEG, J. High Energy Phys. 08 (2018) 205.

[14] T. Melia, P. Nason, R. Rontsch, and G. Zanderighi, W^+W^-, WZ and ZZ production in the POWHEG BOX, J. High Energy Phys. 11 (2011) 078.

[15] P. Nason and G. Zanderighi, W^+W^-, WZ and ZZ production in the POWHEG-BOX-V2, Eur. Phys. J. C **74**, 2702 (2014).

[16] G. Luisoni, P. Nason, C. Oleari, and F. Tramontano, $HW^{\pm}/HZ + 0$ and 1 jet at NLO with the POWHEG BOX interfaced to GoSam and their merging within MiNLO, J. High Energy Phys. 10 (2013) 083.

[17] S. Frixione, P. Nason, and C. Oleari, Matching NLO QCD computations with Parton Shower simulations: The POWHEG method, J. High Energy Phys. 11 (2007) 070.

[18] S. Alioli, P. Nason, C. Oleari, and E. Re, A general framework for implementing NLO calculations in shower Monte Carlo programs: The POWHEG BOX, J. High Energy Phys. 06 (2010) 043.

[19] J. Ohnemus, An order α_s calculation of hadronic W^-W^+ production, Phys. Rev. D **44**, 1403 (1991).

[20] J. Ohnemus, An order α_s calculation of hadronic $W^{\pm}Z$ production, Phys. Rev. D **44**, 3477 (1991).

[21] S. Frixione, P. Nason, and G. Ridolfi, Strong corrections to WZ production at hadron colliders, Nucl. Phys. **B383**, 3 (1992).

[22] J. Ohnemus, Hadronic ZZ, W^-W^+, and $W^{\pm}Z$ production with QCD corrections and leptonic decays, Phys. Rev. D **50**, 1931 (1994).

[23] L. J. Dixon, Z. Kunszt, and A. Signer, Helicity amplitudes for O(α_s) production of W^+W^-, $W^{\pm}Z$, ZZ, $W^{\pm}\gamma$, or $Z\gamma$ pairs at hadron colliders, Nucl. Phys. **B531**, 3 (1998).

[24] J. M. Campbell and R. K. Ellis, An update on vector boson pair production at hadron colliders, Phys. Rev. D **60**, 113006 (1999).

[25] J. M. Campbell, R. K. Ellis, and C. Williams, Vector boson pair production at the LHC, J. High Energy Phys. 07 (2011) 018.

[26] T. Han and S. Willenbrock, QCD correction to the $pp \rightarrow WH$ and ZH total cross-sections, Phys. Lett. B **273,** 167 (1991).

[27] J. Ohnemus and W. J. Stirling, Order α_s corrections to the differential cross-section for the WH intermediate mass Higgs signal, Phys. Rev. D **47,** 2722 (1993).

[28] H. Baer, B. Bailey, and J. F. Owens, $\mathcal{O}(\alpha_s)$ Monte Carlo approach to W + Higgs associated production at hadron supercolliders, Phys. Rev. D **47,** 2730 (1993).

[29] A. Stange, W. J. Marciano, and S. Willenbrock, Associated production of Higgs and weak bosons, with $H \rightarrow b\bar{b}$, at hadron colliders, Phys. Rev. D **50,** 4491 (1994).

[30] C. Degrande, B. Fuks, K. Mawatari, K. Mimasu, and V. Sanz, Electroweak Higgs boson production in the Standard Model effective field theory beyond leading order in QCD, Eur. Phys. J. C **77,** 262 (2017).

[31] S. Banerjee, R. S. Gupta, J. Y. Reiness, S. Seth, and M. Spannowsky, Towards the ultimate differential SMEFT analysis, arXiv:1912.07628.

[32] T. Gehrmann, M. Grazzini, S. Kallweit, P. Maierhofer, A. von Manteuffel, S. Pozzorini, D. Rathlev, and L. Tancredi, W^+W^- Production at Hadron Colliders in Next to Next to Leading Order QCD, Phys. Rev. Lett. **113,** 212001 (2014).

[33] F. Caola, K. Melnikov, R. Rontsch, and L. Tancredi, QCD corrections to W^+W^- production through gluon fusion, Phys. Lett. B **754,** 275 (2016).

[34] M. Grazzini, S. Kallweit, D. Rathlev, and M. Wiesemann, $W^\pm Z$ production at hadron colliders in NNLO QCD, Phys. Lett. B **761,** 179 (2016).

[35] O. Brein, A. Djouadi, and R. Harlander, NNLO QCD corrections to the Higgs-strahlung processes at hadron colliders, Phys. Lett. B **579,** 149 (2004).

[36] G. Ferrera, M. Grazzini, and F. Tramontano, Associated WH Production at Hadron Colliders: A Fully Exclusive QCD Calculation at NNLO, Phys. Rev. Lett. **107,** 152003 (2011).

[37] G. Ferrera, M. Grazzini, and F. Tramontano, Associated ZH production at hadron colliders: The fully differential NNLO QCD calculation, Phys. Lett. B **740,** 51 (2015).

[38] J. M. Campbell, R. K. Ellis, and C. Williams, Associated production of a Higgs boson at NNLO, J. High Energy Phys. 06 (2016) 179.

[39] J. Baglio, L. D. Ninh, and M. M. Weber, Massive gauge boson pair production at the LHC: A next-to-leading order story, Phys. Rev. D **88,** 113005 (2013); **94,** 099902(E) (2016).

[40] A. Bierweiler, T. Kasprzik, and J. H. Kuhn, Vector-boson pair production at the LHC to $\mathcal{O}(\alpha^3)$ accuracy, J. High Energy Phys. 12 (2013) 071.

[41] M. Billoni, S. Dittmaier, B. Jager, and C. Speckner, Next-to-leading order electroweak corrections to $pp \rightarrow W^+W^- \rightarrow 4$ leptons at the LHC in double-pole approximation, J. High Energy Phys. 12 (2013) 043.

[42] B. Biedermann, M. Billoni, A. Denner, S. Dittmaier, L. Hofer, B. Jäger, and L. Salfelder, Next-to-leading-order electroweak corrections to $pp \rightarrow W^+W^- \rightarrow 4$ leptons at the LHC, J. High Energy Phys. 06 (2016) 065.

[43] B. Biedermann, A. Denner, and L. Hofer, Next-to-leading-order electroweak corrections to the production of three charged leptons plus missing energy at the LHC, J. High Energy Phys. 10 (2017) 043.

[44] J. Baglio and N. Le Duc, Fiducial polarization observables in hadronic WZ production: A next-to-leading order QCD + EW study, J. High Energy Phys. 04 (2019) 065.

[45] M. Grazzini, S. Kallweit, J. M. Lindert, S. Pozzorini, and M. Wiesemann, NNLO QCD + NLO EW with Matrix + OpenLoops: Precise predictions for vector-boson pair production, J. High Energy Phys. 02 (2020) 087.

[46] A. Denner, S. Dittmaier, S. Kallweit, and A. Muck, Electroweak corrections to Higgs-strahlung off W/Z bosons at the Tevatron and the LHC with HAWK, J. High Energy Phys. 03 (2012) 075.

[47] K. Hagiwara, R. D. Peccei, D. Zeppenfeld, and K. Hikasa, Probing the weak Boson sector in $e^+e^- \rightarrow W^+W^-$, Nucl. Phys. **B282,** 253 (1987).

[48] K. Hagiwara, R. Szalapski, and D. Zeppenfeld, Anomalous Higgs boson production and decay, Phys. Lett. B **318,** 155 (1993).

[49] U. Baur, T. Han, and J. Ohnemus, WZ production at hadron colliders: Effects of nonstandard WWZ couplings and QCD corrections, Phys. Rev. D **51,** 3381 (1995).

[50] U. Baur, T. Han, and J. Ohnemus, QCD corrections and nonstandard three vector boson couplings in W^+W^- production at hadron colliders, Phys. Rev. D **53,** 1098 (1996).

[51] L. J. Dixon, Z. Kunszt, and A. Signer, Vector boson pair production in hadronic collisions at order α_s: Lepton correlations and anomalous couplings, Phys. Rev. D **60,** 114037 (1999).

[52] M. Chiesa, A. Denner, and J.-N. Lang, Anomalous triple-gauge-boson interactions in vector-boson pair production with RECOLA2, Eur. Phys. J. C **78,** 467 (2018).

[53] F. Campanario, R. Roth, and D. Zeppenfeld, QCD radiation in WH and WZ production and anomalous coupling measurements, Phys. Rev. D **91,** 054039 (2015).

[54] F. Granata, J. M. Lindert, C. Oleari, and S. Pozzorini, NLO QCD + EW predictions for HV and HV + jet production including parton-shower effects, J. High Energy Phys. 09 (2017) 012.

[55] A. Azatov, D. Barducci, and E. Venturini, Precision diboson measurements at hadron colliders, J. High Energy Phys. 04 (2019) 075.

[56] R. Contino, A. Falkowski, F. Goertz, C. Grojean, and F. Riva, On the validity of the effective field theory approach to SM precision tests, J. High Energy Phys. 07 (2016) 144.

[57] C. Hays, A. Martin, V. Sanz, and J. Setford, On the impact of dimension-eight SMEFT operators on Higgs measurements, J. High Energy Phys. 02 (2019) 123.

[58] S. Alte, M. Konig, and W. Shepherd, Consistent searches for SMEFT effects in non-resonant Dilepton events, J. High Energy Phys. 07 (2019) 144.

[59] A. Falkowski, M. Gonzalez-Alonso, A. Greljo, and D. Marzocca, Global Constraints on Anomalous Triple Gauge Couplings in Effective Field Theory Approach, Phys. Rev. Lett. **116,** 011801 (2016).

[60] R. Franceschini, G. Panico, A. Pomarol, F. Riva, and A. Wulzer, Electroweak precision tests in high-energy Diboson processes, J. High Energy Phys. 02 (2018) 111.

[61] D. Liu and L.-T. Wang, Prospects for precision measurement of diboson processes in the semileptonic decay channel in future LHC runs, Phys. Rev. D **99,** 055001 (2019).

[62] S. Banerjee, C. Englert, R. S. Gupta, and M. Spannowsky, Probing electroweak precision physics via boosted Higgs-strahlung at the LHC, Phys. Rev. D **98,** 095012 (2018).

[63] S. Banerjee, R. S. Gupta, J. Y. Reiness, and M. Spannowsky, Resolving the tensor structure of the Higgs coupling to Z-bosons via Higgs-strahlung, Phys. Rev. D **100,** 115004 (2019).

[64] A. Falkowski, B. Fuks, K. Mawatari, K. Mimasu, F. Riva, and V. Sanz, Rosetta: An operator basis translator for Standard Model effective field theory, Eur. Phys. J. C **75,** 583 (2015).

[65] A. Dedes, W. Materkowska, M. Paraskevas, J. Rosiek, and K. Suxho, Feynman rules for the Standard Model effective field theory in R$_\xi$-gauges, J. High Energy Phys. 06 (2017) 143.

[66] I. Brivio and M. Trott, Scheming in the SMEFT... and a reparameterization invariance!, J. High Energy Phys. 07 (2017) 148; 05 (2018) 136(A).

[67] E. E. Jenkins, A. V. Manohar, and P. Stoffer, Low-energy effective field theory below the electroweak scale: Operators and matching, J. High Energy Phys. 03 (2018) 016.

[68] Z. Zhang, Time to Go Beyond Triple-Gauge-Boson-Coupling Interpretation of W Pair Production, Phys. Rev. Lett. **118,** 011803 (2017).

[69] L. Berthier and M. Trott, Towards consistent electroweak precision data constraints in the SMEFT, J. High Energy Phys. 05 (2015) 024.

[70] E. da Silva Almeida, N. Rosa-Agostinho, O. J. Eboli, and M. Gonzalez-Garcia, Light-quark dipole operators at the LHC, Phys. Rev. D **100,** 013003 (2019).

[71] R. S. Gupta, A. Pomarol, and F. Riva, Leading effects beyond the standard model, Phys. Rev. D **91,** 035001 (2015).

[72] A. Falkowski, Effective field theory approach to LHC Higgs data, Pramana **87,** 39 (2016).

[73] M. Tanabashi *et al.* (Particle Data Group), Review of particle physics, Phys. Rev. D **98,** 030001 (2018).

[74] S. Alioli, V. Cirigliano, W. Dekens, J. de Vries, and E. Mereghetti, Right-handed charged currents in the era of the Large Hadron Collider, J. High Energy Phys. 05 (2017) 086.

[75] C. Schmidt, J. Pumplin, D. Stump, and C. P. Yuan, CT14QED parton distribution functions from isolated photon production in deep inelastic scattering, Phys. Rev. D **93,** 114015 (2016).

[76] U. Baur, T. Han, and J. Ohnemus, Amplitude Zeros in $W^\pm Z$ Production, Phys. Rev. Lett. **72,** 3941 (1994).

[77] G. Panico, F. Riva, and A. Wulzer, Diboson interference resurrection, Phys. Lett. B **776,** 473 (2018).

[78] J. Brehmer, S. Dawson, S. Homiller, F. Kling, and T. Plehn, Benchmarking simplified template cross sections in WH production, J. High Energy Phys. 11 (2019) 034.

[79] M. Aaboud *et al.* (ATLAS Collaboration), Measurement of $W^\pm Z$ production cross sections and gauge boson polarisation in pp collisions at $\sqrt{s} = 13$ TeV with the ATLAS detector, Eur. Phys. J. C **79,** 535 (2019).

[80] Z. Bern *et al.*, Left-handed W Bosons at the LHC, Phys. Rev. D **84,** 034008 (2011).

[81] A. Falkowski, M. Gonzalez-Alonso, A. Greljo, D. Marzocca, and M. Son, Anomalous triple gauge couplings in the effective field theory approach at the LHC, J. High Energy Phys. 02 (2017) 115.

[82] R. Rahaman and R. K. Singh, Unravelling the anomalous gauge boson couplings in $ZW^\pm$ production at the LHC and the role of spin-1 polarisations, J. High Energy Phys. 04 (2020) 075.

[83] L. J. Dixon and Y. Shadmi, Testing gluon self-interactions in three-jet events at hadron colliders, Nucl. Phys. **B423,** 3 (1994); **B452,** 724(E) (1995).

[84] A. Azatov, J. Elias-Miro, Y. Reyimuaji, and E. Venturini, Novel measurements of anomalous triple gauge couplings for the LHC, J. High Energy Phys. 10 (2017) 027.

[85] M. Aaboud *et al.* (ATLAS Collaboration), Measurement of VH, H → b$\bar{\text{b}}$ production as a function of the vector-boson transverse momentum in 13 TeV pp collisions with the ATLAS detector, J. High Energy Phys. 05 (2019) 141.

[86] G. Aad *et al.* (ATLAS Collaboration), Measurement of total and differential $W^+ W^-$ production cross sections in proton-proton collisions at $\sqrt{s} = 8$ TeV with the ATLAS detector and limits on anomalous triple-gauge-boson couplings, J. High Energy Phys. 09 (2016) 029.

[87] M. Aaboud *et al.* (ATLAS Collaboration), Measurement of fiducial and differential $W^+ W^-$ production cross-sections at $\sqrt{s} = 13$ TeV with the ATLAS detector, Eur. Phys. J. C **79,** 884 (2019).

[88] G. Aad *et al.* (ATLAS Collaboration), Measurements of $W^\pm Z$ production cross sections in pp collisions at $\sqrt{s} = 8$ TeV with the ATLAS detector and limits on anomalous gauge boson self-couplings, Phys. Rev. D **93,** 092004 (2016).

[89] V. Khachatryan *et al.* (CMS Collaboration), Measurement of the WZ production cross section in pp collisions at $\sqrt{s} = 7$ and 8 TeV and search for anomalous triple gauge couplings at $\sqrt{s} = 8$ TeV, Eur. Phys. J. C **77,** 236 (2017).

[90] A. M. Sirunyan *et al.* (CMS Collaboration), Measurements of the pp → WZ inclusive and differential production cross section and constraints on charged anomalous triple gauge couplings at $\sqrt{s} = 13$ TeV, J. High Energy Phys. 04 (2019) 122.

[91] A. Falkowski and F. Riva, Model-independent precision constraints on dimension-6 operators, J. High Energy Phys. 02 (2015) 039.

[92] S. Dawson and P. P. Giardino, Electroweak and QCD corrections to Z and W pole observables in the Standard Model EFT, Phys. Rev. D **101,** 013001 (2020).

[93] https://quark.phy.bnl.gov/Digital_Data_Archive/dawson/VV_20